Chapter 2

Experimental bounds on sterile neutrino mixing angles

2.1 Introduction

As discussed in the Introduction (Section 1.2.1), neutrinos are massive and can change their *flavours* while propagating (see e.g. [104] for a review). This is one of the few firmly established phenomena beyond the Standard Model of particle physics. While the absolute scale of neutrino masses is not determined yet, combinations of direct measurements and oscillations experiments put the sum of their masses below 2 eV [105] while from the cosmological data one can infer an upper bound of 0.58 eV at 95% CL [106].

Thus the neutrinos are massive but their mass is at least million times smaller than the masses of other fermions.

A traditional explanation of *both* neutrino oscillations *and* the smallness of neutrino masses is provided by the *see-saw mechanism* [46, 47, 48, 49], see also Section 1.3. It assumes the existence of several *right-handed neutrinos* (Fig. 1.3) coupled to their Standard Model counterparts via the Yukawa interaction, providing the Dirac masses, M_{D}, for neutrinos. The Yukawa interaction terms dictate the SM charges of the right-handed particles: they turn out to carry no electric, weak and strong charges; therefore they are often termed "singlet," or "sterile" fermions. Sterile neutrinos can thus have Majorana masses, M_s, consistent with the gauge symmetries of the Standard Model. If the Majorana masses are much larger than the Dirac ones, the *type I seesaw formula* (1.10) holds [46, 47, 48, 49]. The masses of sterile neutrinos are much heavier than the active neutrino masses as a consequence of this formula. This creates quite a unique situation: the left-chiral and right-chiral counterparts behave as two distinct particles with different masses and interaction strengths.

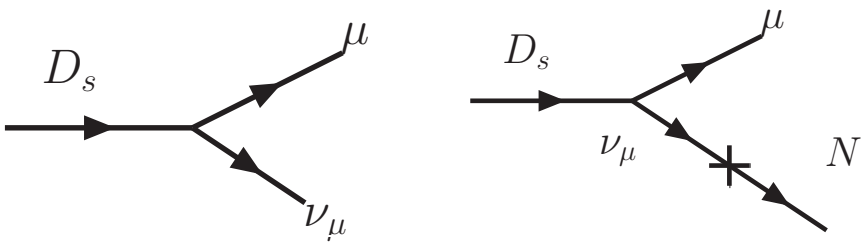

Figure 2.1: Leptonic decay of the D_s meson, $D_s \to \mu^+ + \nu_\mu$ (left) is accompanied by the decay to sterile neutrino, N, $D_s \to \mu^+ + N$ (right). On the right, the weak eigenstate ν_μ is converted to the mass eigenstate of N. The relative probability of the left and right processes is different by $\vartheta^2 = |M_D/M_s|^2$.

As we have argued in Sec. 1.3, although sterile neutrinos are neutral with respect to the SM charges, they interact with the SM matter through mixing with active neutrinos, and can be detected (See Fig. 2.1). This opens a possibility to search for sterile neutrinos at particle physics experiments.

Any process with active neutrino in the initial or final state **has its counterpart with sterile neutrino** (if kinematically allowed) with the probability suppressed by the squared mixing angle ϑ^2.

2.1.1 Previous bounds on sterile neutrino interactions

Numerous searches for sterile neutrinos in the mass range up to $\sim$ 500 GeV had been performed in the past (see the corresponding section in Particle Data Group [105],[1] see also [107, 101] and refs. therein). These searches provided *upper bounds* on the strength of interaction of these neutral leptons with the SM neutrinos of different flavours – active-sterile neutrino *mixing angles* for sterile neutrino with the mass M_s.[2] These bounds then can be interpreted as *lower bounds* on the lifetime of sterile neutrinos τ_s via

$$\tau_s^{-1} = \frac{G_F^2 M_s^5}{96\pi^3} \sum_\alpha \vartheta_\alpha^2 \sum_X B_X^{(\alpha)}, \tag{2.1}$$

where the sum runs over various kinematically allowed decay modes X of sterile neutrinos. The coefficients $B_X^{(\alpha)}$ depend on the sterile neutrino mass. For example,

[1] http://pdglive.lbl.gov/Rsummary.brl?nodein=S077&inscript=Y

[2] Here and below we use the letter ϑ for *active-sterile mixing angles* (defined by Eq. (2.12) below) while reserving θ_{12}, θ_{13} and θ_{23} for the measured parameters of the active neutrinos matrix $\hat{m}_\nu$. These quantities ϑ_α are often denoted $|V_{4\alpha}|^2$ or $|U_{x\alpha}|^2$ in the experimental papers, to which we refer. Here and below the Greek letters α, β are flavour index e, μ, τ and $i, j = 1, 2, 3$ denote active neutrino mass eigenstates.

if sterile neutrino is lighter than two electron masses, then the only kinematically allowed decay mode is $N \to \nu\nu\bar{\nu}$, and

$$B^e_{\nu\nu\nu} = B^\mu_{\nu\nu\nu} = B^\tau_{\nu\nu\nu} = 1 \tag{2.2}$$

For higher masses, the coefficients $B_X^{(\alpha)}$ can be read from [99].

The lower bound on the lifetime τ_s is usually dominated by the least constrained mixing angle, which happens to be ϑ_τ^2 (as will be shown later). This bound can be made *stronger* if one assumes that the same particles are also responsible for the neutrino oscillations. The see-saw formula (2.3) limits (at least partially) possible values of ratios of the mixing angles $\vartheta_\alpha^2/\vartheta_\beta^2$. In the simplest case when only two sterile neutrinos are present (the minimal number, required to explain two observed neutrino mass differences) the ratios of mixing angles varies within a limited range, see e.g. [108, 109]. While this range can be several orders of magnitude large (owing to our ignorance of certain oscillation parameters, such as e.g. a CP-violating phase [108, 109]), the implied (lower) bounds on the lifetime become much stronger, essentially being determined by the *strongest*, rather than the weakest direct bound on ϑ_α.

The structure of this Chapter

In this Chapter we summarize restrictions on sterile neutrino lifetime in view of the recent results of the Daya Bay [10] and RENO [9] collaborations, that measured a non-zero mixing angle θ_{13} (see also [13, 12]). We demonstrate that in the case when there are only two sterile neutrinos, responsible for the observed neutrino oscillations, the oscillation data allow for such a choice of the active-sterile Yukawa couplings that the mixing of sterile neutrinos with any given flavour can be strongly suppressed. This happens *only* for a non-zero values of θ_{13}, in the range consistent with the current measurements [110, 111, 10, 9]. The results of this Chapter partially overlap with [112] (also [113]), and we make the comparison with the previous works in the corresponding places.

This Chapter is organized as follows: in Section 2.2 we briefly describe the model of sterile neutrinos that we use. We then investigate the relations between different mixing angles imposed by the see-saw mechanism and demonstrate that the mixing with any flavour ϑ_α^2 can become suppressed (Section 2.3). Section 2.4 is devoted to the overview of the experiments, searching for sterile neutrinos with the masses below 2 GeV, and the way one should interpret their results to apply to the see-saw models that we study. Section 2.5 summarizes our revised bounds on mixing angles and translates them into the resulting constraints on sterile neutrino lifetime (Figs. 2.8). We conclude in Section 2.6, discussing implications of our results and confronting them with the bounds from primordial nucleosynthesis.

2.2 Sterile neutrino Lagrangian

The minimal way to add sterile neutrinos to the Standard Model is provided by the Type I see-saw model (Eq. (1.9) in Section 1.3), see also [46, 47, 48, 49], [114, 115, 116, 117] and refs. therein). This model contains $\mathcal{N}$ new fermions N_I — sterile neutrinos. *How many of them can there be?*

The masses of the active neutrinos are given by the seesaw relation

$$\hat{m}_\nu = -M_{\text{D}} M_s^{-1} M_{\text{D}}^T, \tag{2.3}$$

where $\hat{m}_\nu$ is a 3×3 matrix of active neutrino masses, mixings, and (possible) CP-violating phases, M_s is the matrix of the Majorana masses of sterile neutrinos N_I and the M_{D} is the usual Dirac mass term coupling active and sterile neutrinos. Formula (1.10) is a particular case of the relation (2.3) for $mathcalN = 3$ and diagonal form of the Majorana matrix M_s.

The number of these singlet fermions must be $\mathcal{N} \geq 2$ to explain the data on neutrino oscillations. In the case of $\mathcal{N} = 2$ there are *11 new parameters* in the Lagrangian (1.9), while the neutrino mass/mixing matrix $\hat{m}_\nu$ has 7 parameters in this case. The situation is even more relaxed for $\mathcal{N} > 2$. The see-saw formula (2.3) does not allow to fix the scale of Majorana and Dirac $M_{\text{D},\alpha I} = F_{\alpha I}\langle\Phi\rangle$ masses.

2.2.1 Two quasi-degenerate sterile neutrinos

In this work we will mostly concentrate on sterile neutrinos with their masses M_s in the MeV–GeV range – the range in which the past direct accelerator searches were the most sensitive. To further simplify our analysis we will concentrate on the case when the masses of both sterile neutrinos are close to each other (so that $\Delta M \ll M_s$). One important example of such model is provided by the *Neutrino Minimal Standard Model* (the νMSM) ([118, 119], see [120] for review). Within the νMSM there are **3** sterile neutrinos, whose masses are roughly of the order of those of other leptons in the Standard Model (see Section 1.3.4). Two of these particles are approximately degenerate in their mass and are responsible for baryogenesis and neutrino oscillations and the third one is playing the role of dark matter. As we have noticed in Section 1.3, the requirement of dark matter stability on cosmological timescales makes its coupling with the Standard Model species so feeble, that it does not contribute significantly to the neutrino oscillation pattern [118, 121]. Therefore, when analyzing neutrino oscillations, the N_1 can be omitted from the Lagrangian and index I in the sums runs through 2 and 3 only. Taking into account that $M_2 \approx M_3 \approx M_s$, we perform a rotation in the space $(N_2, N_3) \to (\boldsymbol{N}_2, \boldsymbol{N}_3)$ such that the Majorana mass term of the see-saw Lagrangian (1.9) is off-diagonal[3]

[3]This parametrization coincides with [109, Eq. (2.1)].

$$\Delta\mathcal{L}^{\nu\text{MSM}}_{N_2,N_3} = i\bar{\boldsymbol{N}}_I\partial\!\!\!/\boldsymbol{N}_I - M_{\text{D},\alpha I}\bar{\nu}_\alpha\boldsymbol{N}_I - M^*_{\text{D},\alpha I}\bar{\boldsymbol{N}}_I\nu_\alpha - M_s\left(\bar{\boldsymbol{N}}^c_2\boldsymbol{N}_3 + \bar{\boldsymbol{N}}_3\boldsymbol{N}^c_2\right) \quad (2.4)$$

In what follows we will abuse the notations and continue to use N_2, N_3 also for the basis of the Lagrangian (2.4).

2.3 Solution of the see-saw equations

In this Section we investigate how mixing angles between active and sterile neutrinos are related to parameters of the observable neutrino matrix $\hat{m}_\nu$. We will demonstrate that the mixing angle ϑ^2_e in the case of normal hierarchy and the mixing angles ϑ^2_μ or ϑ^2_τ in the case of inverted hierarchy, can become suppressed as we vary the parameters of the neutrino matrix away from their best-fit values (but within the experimentally allowed 3σ bounds).

2.3.1 Parametrization of the Dirac mass matrix

We use the Pontecorvo–Maki–Nakagawa–Sakata (PMNS) parametrization of the neutrino matrix $\hat{m}_\nu$ (see e.g. Eqs.(2.10) and (2.12) of [104])

$$\hat{m}_\nu = V^*\text{diag}(m_1e^{-2i\zeta},\ m_2e^{-2i\xi},\ m_3)V^\dagger\ , \quad (2.5)$$

where V is the unitary matrix, whose explicit standard form is (cf. e.g. [104])

$$V = \begin{pmatrix} 1 & 0 & 0 \\ 0 & c_{23} & s_{23} \\ 0 & -s_{23} & c_{23} \end{pmatrix}\begin{pmatrix} c_{13} & 0 & s_{13} \\ 0 & e^{i\phi} & 0 \\ -s_{13} & 0 & c_{13} \end{pmatrix}\begin{pmatrix} c_{12} & s_{12} & 0 \\ -s_{12} & c_{12} & 0 \\ 0 & 0 & 1 \end{pmatrix}$$

$$= \begin{pmatrix} c_{12}c_{13} & c_{13}s_{12} & s_{13} \\ -c_{23}s_{12}e^{i\phi} - c_{12}s_{13}s_{23} & c_{12}c_{23}e^{i\phi} - s_{12}s_{13}s_{23} & c_{13}s_{23} \\ s_{23}s_{12}e^{i\phi} - c_{12}c_{23}s_{13} & -c_{12}s_{23}e^{i\phi} - c_{23}s_{12}s_{13} & c_{13}c_{23} \end{pmatrix}\ . \quad (2.6)$$

where $c_{ij} = \cos\theta_{ij}$, and $s_{ij} = \sin\theta_{ij}$.

Redefining a Dirac mass matrix as[4]

$$M_\text{D} \to \tilde{M}_\text{D} \equiv V^T M_\text{D}\ , \quad (2.7)$$

we can rewrite the see-saw relation (2.3) in the following form:

$$\text{diag}(m_1e^{-2i\zeta},\ m_2e^{-2i\xi},\ m_3)_{ij} = -\frac{\tilde{M}_{\text{D},i2}\tilde{M}_{\text{D},j3} + \tilde{M}_{\text{D},i3}\tilde{M}_{\text{D},j2}}{M_s}\ , \quad (2.8)$$

[4]The Dirac matrix $\tilde{M}_\text{D}$ has indexes $I = 2,3$ and $i,j = 1,2,3$, which correspond to sterile and active neutrino mass eigenstates, respectively.

Normal hierarchy		Inverted hierarchy	
Δm^2_{21}	$(7.09 - 8.19) \times 10^{-5}\,\mathrm{eV}^2$		
Δm^2_{31}	$(2.14 - 2.76) \times 10^{-3}\,\mathrm{eV}^2$	Δm^2_{13}	$(2.13 - 2.67) \times 10^{-3}\,\mathrm{eV}^2$
$\sin^2\theta_{12}$	$0.27 - 0.36$		
$\sin^2\theta_{23}$	$0.39 - 0.64$		
$\sin^2\theta_{13}$	$0.010 - 0.038$ $(0.013 - 0.040)$		

Table 2.1: The 3σ bounds on the parameters of the mass matrix $\hat{m}_\nu$, adopted from [123, 111, 10, 9]. Here $\Delta m^2_{ij} = m^2_i - m^2_j$. The boundaries for inverted hierarchy are the same as for the normal one, unless written explicitly. The range of $\sin^2\theta_{13}$ is taken from the data of the Daya Bay experiment [10] (the values in parentheses – from RENO [9]).

The rank of the active neutrino mass matrix $\mathcal{M}_\nu$ is 2 in the case of two sterile neutrinos, meaning that one of the masses m_i is zero.

In neutrino oscillations, only two independent combinations $m^2_2 - m^2_1$ and $m^2_3 - m^2_1$ of the active neutrino mass eigenvalues m_1, m_2, m_3 are measured. Based on this, two choices of "hierarchies" are possible, which cannot be distinguished from neutrino oscillation data alone. The first one is called *normal hierarchy* (NH) and corresponds to $0 \leq m_1 < m_2 < m_3$. The second one is called *inverted hierarchy* (IH) and is realized for $0 \leq m_3 < m_1 < m_2$.

Once the mass M_s is fixed, the solutions of Eq. (2.8) contain one unknown complex parameter, z. Its presence reflects a symmetry of the see-saw relation (2.8) under the change $(\tilde{M}_{\mathrm{D},i2}, \tilde{M}_{\mathrm{D},i3}) \to (z\tilde{M}_{\mathrm{D},i2}, z^{-1}\tilde{M}_{\mathrm{D},i3})$ [122]. It is this freedom that does not allow to fix the absolute scale of $\tilde{M}_\mathrm{D}$ (i.e. the value of ϑ^2) even if M_s is chosen.

The change $z \to z^{-1}$ is equivalent to the redefinition of $N_2 \to N_3$, $N_3 \to N_2$ together with shift of the Majorana phase $\xi \to \xi + \pi$ in (2.8). Therefore in subsequent analysis we will choose $|z| \geq 1$ without the loss of generality.

2.3.2 Normal hierarchy

For normal hierarchy the explicit see-saw relation is

$$\mathrm{diag}(0,\ m_2 e^{-2i\xi},\ m_3)_{ij} = -\frac{\tilde{M}_{\mathrm{D},i2}\tilde{M}_{\mathrm{D},j3} + \tilde{M}_{\mathrm{D},i3}\tilde{M}_{\mathrm{D},j2}}{M_s}\ . \tag{2.9}$$

Diagonal components of this matrix equation give

$$\tilde{M}_{\mathrm{D},12}\tilde{M}_{\mathrm{D},13} = 0,\ \ \tilde{M}_{\mathrm{D},22}\tilde{M}_{\mathrm{D},23} = \frac{1}{2}m_2 M_s e^{-2i\xi},\ \ \tilde{M}_{\mathrm{D},32}\tilde{M}_{\mathrm{D},33} = \frac{1}{2}m_3 M_s\ . \tag{2.10}$$

Using $m_2, m_3 \neq 0$ we find that $\tilde{M}_{\mathrm{D},22}$, $\tilde{M}_{\mathrm{D},23}$, $\tilde{M}_{\mathrm{D},32}$, $\tilde{M}_{\mathrm{D},33}$ are *all* non-zero. Analysis of non-diagonal terms reveals that *both* $\tilde{M}_{\mathrm{D},12}$ and $\tilde{M}_{\mathrm{D},13}$ are zero and

there are two general solutions (c.f. [122]):

$$\tilde{M}^{\pm}_{\mathrm{D},i2} = iz\sqrt{\frac{M_s}{2}}(0,\ \pm ie^{-i\xi}\sqrt{m_2},\ \sqrt{m_3}),\ \ \tilde{M}^{\pm}_{\mathrm{D},i3} = iz^{-1}\sqrt{\frac{M_s}{2}}(0,\ \mp ie^{-i\xi}\sqrt{m_2},\ \sqrt{m_3})\ . \tag{2.11}$$

The solution $\tilde{M}^{+}_{\mathrm{D}}$ with $\xi = \psi + \pi$ equals to $\tilde{M}^{-}_{\mathrm{D}}$ with $\xi = \psi$. It allows us to consider only one solution $\tilde{M}^{+}_{D}$ on the interval $0 \leq \xi < 2\pi$. In what follows we therefore omit the superscript $+$.[5]

The mixing angles of the active-sterile neutrinos are defined as follows:

$$2\vartheta^2_\alpha \equiv \sum_I |(M_{\mathrm{D}}M_s^{-1})_{\alpha I}|^2 = \sum_I |(V^*\tilde{M}_{\mathrm{D}}M_s^{-1})_{\alpha I}|^2 = \frac{1}{M_s^2}\sum_I |(V^*\tilde{M}_{\mathrm{D}})_{\alpha I}|^2\ . \tag{2.12}$$

Inserting the explicit solution (2.11) for $\tilde{M}_{\mathrm{D}}$ results in

$$\vartheta^2_\alpha = \frac{|z|^2}{4M_s}\left|\sqrt{m_3}V_{\alpha 3} - ie^{i\xi}\sqrt{m_2}V_{\alpha 2}\right|^2 + \frac{1}{4M_s|z|^2}\left|\sqrt{m_3}V_{\alpha 3} + ie^{i\xi}\sqrt{m_2}V_{\alpha 2}\right|^2 . \tag{2.13}$$

For $|z| \gg 1$ the contribution of $\tilde{M}_{\mathrm{D},i3}$ is suppressed compared with that of $\tilde{M}_{\mathrm{D},i2}$ and therefore we neglect the former (we will comment below on the case $|z| \gtrsim 1$).

As the value of the Majorana phase ξ is undetermined experimentally, the condition $\vartheta_\alpha = 0$ is satisfied iff $m_3|V_{\alpha 3}|^2 = m_2|V_{\alpha 2}|^2$ (we neglect second term on the r.h.s. of (2.13)). For the electron flavour ($\alpha = e$) it translates into

$$\sin^2\theta_{12}\frac{m_2}{m_3} = \tan^2\theta_{13}, \tag{2.14}$$

which, in principle, can be satisfied only for non-zero θ_{13}. This result has been already obtained in [112].

The bounds on the parameters of the mass matrix $\hat{m}_\nu$ at the 3σ level that we use are shown in Table 2.1. Note that in the present analysis we do not take into account statistical correlations between different oscillation parameters, allowing them to vary independently within their 3σ intervals. Consequently, we obtain the 3σ intervals for the combinations of parameters, entering Eq. (2.14)[6]:

$$\begin{array}{rcccl} 0.043 & < & \sin^2\theta_{12}\frac{m_2}{m_3} & < & 0.070, \\ 0.010(0.014) & < & \tan^2\theta_{13} & < & 0.039(0.042), \end{array} \tag{2.15}$$

[5] Unlike the parametrizations used e.g. in Ref. [124, 122, 112] this way of parametrizing the solution of the see-saw equations shows that there is only one branch of solutions, with all other related to it via redefinitions $N_2 \leftrightarrow N_3$ and shift of the Majorana phases. In particular in the parametrization we used it is much easier to analyze whether mixing angles become zero. The relation $|z| = \exp(\mathrm{Im}\,\omega)$ holds, where the parameter ω was employed in [112].

[6] Throughout this Chapter whenever two numbers are given instead of one, the first is based on the results of the Daya Bay experiment [10], and the second one (in parentheses) is obtained based on the result of application of the RENO bounds [9] (see Table 2.1).

They imply that the relation (2.14) *does not* hold exactly for the neutrino oscillation parameters, presented in Table 2.1. Therefore the mixing angle ϑ_e^2 cannot become zero, but has a non-trivial lower bound. To find the minimal value that it can reach, we consider the ratio of the angles $\vartheta_e^2/(\vartheta_e^2+\vartheta_\mu^2+\vartheta_\tau^2)$. Due to the unitarity of V, the denominator is

$$\sum_\alpha \vartheta_\alpha^2 \approx \frac{1}{2M_s^2}\sum_{\alpha,\beta,\gamma} V^*_{\alpha\beta}\tilde{M}_{\text{D},\beta 2}V_{\alpha\gamma}\tilde{M}^*_{\text{D},\gamma 2} = \frac{1}{2M_s^2}\sum_\beta \tilde{|}M_{\text{D},\beta 2}|^2 = \frac{|z|^2}{4M_s}(m_2+m_3). \tag{2.16}$$

Let us denote the ratio of the mixing of sterile neutrinos with one flavour to the sum of all mixings by T_α,

$$T_\alpha \equiv \frac{\vartheta_\alpha^2}{\sum\limits_\beta \vartheta_\beta^2}. \tag{2.17}$$

Then we get the following expression for T_e:

$$T_e = \frac{|ie^{i\xi}c_{13}s_{12}\sqrt{\frac{m_2}{m_3}} - s_{13}|^2}{1+\frac{m_2}{m_3}}. \tag{2.18}$$

The minimum is achieved if we push θ_{12} and Δm^2_{21} to their 3σ lower boundaries, θ_{13} and Δm^2_{31} to their upper boundaries, and choose $\xi = -\pi/2$. The maximum is achieved when we set Δm^2_{31} equal to its lower bound, θ_{13}, θ_{12} and Δm^2_{21} to their upper bounds, and by choosing the Majorana phase $\alpha = \pi/2$. The bounds on T_e from Table 2.2 translate into the bound for the muon and tau flavours combined:

$$0.83 \leq T_\mu + T_\tau. \tag{2.19}$$

The minimum and maximum of different T_α are listed in the Table 2.2 and in Fig. 2.2.

This analysis was conducted in approximation of large $|z|$. See Sec. 2.3.4 for the account of finite-$|z|$ effects.

2.3.3 Inverted hierarchy

Similarly to the previous case, for the inverted hierarchy we get a solution of the see-saw equations (2.8)

$$\tilde{M}_{\text{D},i2} = iz\sqrt{\frac{M_s}{2}}(e^{-i\zeta}\sqrt{m_1},\ ie^{-i\xi}\sqrt{m_2},\ 0),\quad \tilde{M}_{\text{D},i3} = iz^{-1}\sqrt{\frac{M_s}{2}}(e^{-i\zeta}\sqrt{m_1},\ -ie^{-i\xi}\sqrt{m_2},\ 0) \tag{2.20}$$

Normal hierarchy	Inverted hierarchy
$T_e \leq 0.15$	$0.02 \leq T_e \leq 0.98$
$0.09 \leq T_\mu \leq 0.89$	$0 \leq T_\mu \leq 0.60$
$0.08 \leq T_\tau \leq 0.88$	2×10^{-4} $(7 \times 10^{-5}) \leq T_\tau \leq 0.62$
The ranges are based on 2σ bounds	

Normal hierarchy	Inverted hierarchy
$T_e \leq 0.17$	$0.02 \leq T_e \leq 0.98$
$0.07 \leq T_\mu \leq 0.92$	$0 \leq T_\mu \leq 0.63$
$0.06 \leq T_\tau \leq 0.90$	$0 \leq T_\tau \leq 0.65$
The ranges are based on 3σ bounds	

Table 2.2: The ratio of the sterile neutrino mixing with a given flavour α to the *sum* of the three mixings, T_α (defined by (2.17)). **Left** table shows the upper and lower values of T_α when parameters of neutrino oscillations are allowed to vary within their 2σ boundaries (taken from [123]). The **right** table shows the results when the parameters of active neutrino oscillations are varied within their 3σ limits (see Table 2.1). For the explanation of the numbers in parentheses, see Footnote 6.

for $0 \leq \xi < 2\pi$. In this case ϑ_μ^2 or ϑ_τ^2 can become very suppressed, as we will show soon.

The mixing angles are

$$\vartheta_\alpha^2 = \frac{|z|^2}{4M_s}\left|\sqrt{m_1}V_{\alpha 1} - ie^{i(\xi-\zeta)}\sqrt{m_2}V_{\alpha 2}\right|^2 + \frac{1}{4M_s|z|^2}\left|\sqrt{m_1}V_{\alpha 1} + ie^{i(\xi-\zeta)}\sqrt{m_2}V_{\alpha 2}\right|^2. \tag{2.21}$$

For $|z| \gg 1$ they can become close to zero only if $\sqrt{m_1}|V_{\alpha 1}| = \sqrt{m_2}|V_{\alpha 2}|$. For $\alpha = \mu$ this condition translates into

$$|\tan\theta_{12} + \sin\theta_{13}\tan\theta_{23}e^{-i\phi}| = \sqrt{\frac{m_2}{m_1}}|1 - \sin\theta_{13}\tan\theta_{12}\tan\theta_{23}e^{-i\phi}|. \tag{2.22}$$

For the parameter set close to the best fit, left-hand side is *less* than the right-hand side, because then $\sin\theta_{13} \approx 0$, while $\tan\theta_{12} < 1$ and $m_1 \approx m_2$. To attain the equality one has to push left-hand side up and the right-hand side down. $\phi = 0$ makes phases of both complex terms inside $|...|$ on the left-hand side equal, thereby the absolute value of their sum becomes maximal. Simultaneously the right-hand side becomes minimal. For this specific choice of the Dirac angle the equality (2.22) turns into

$$\frac{\sqrt{\frac{m_2}{m_1}} - \tan\theta_{12}}{\sqrt{\frac{m_2}{m_1}}\tan\theta_{12} + 1} = \sin\theta_{13}\tan\theta_{23}. \tag{2.23}$$

The 3σ bounds for inverted hierarchy in general are the same as for the normal one (see Table 2.1) with the exception of the "atmospheric" mass difference, that slightly differs. Using these values we find

$$0.14 < \frac{\sqrt{\frac{m_2}{m_1}} - \tan\theta_{12}}{\sqrt{\frac{m_2}{m_1}}\tan\theta_{12} + 1} < 0.24, \quad 0.08\ (0.09) < \sin\theta_{13}\tan\theta_{23} < 0.26. \tag{2.24}$$

We see that two regions overlap, therefore the relation (2.22) can be satisfied and ϑ_μ^2 can be zero in a wide region of values of the parameters of the neutrino oscillation matrix. See, however, Sec. 2.3.5 below.

Similarly, the condition $\vartheta_\tau = 0$ (for $\phi = \pi$) translates into

$$\frac{\sqrt{\frac{m_2}{m_1}} - \tan\theta_{12}}{\sqrt{\frac{m_2}{m_1}}\tan\theta_{12} + 1} = \sin\theta_{13}\cot\theta_{23}, \tag{2.25}$$

and can be satisfied, because the quantity on the right hand side varies from 0.07 (0.09) to 0.24 (0.25), well within the range of (2.24).[7]

On the other hand, ϑ_e can be zero only if

$$\cot\theta_{12} = \sqrt{\frac{m_2}{m_1}} \tag{2.26}$$

can be realized. The left hand side is always larger than the right hand side (within the 3σ region), therefore no ϑ_e suppression can occur. However it is important to know what minimal value this mixing angle can reach. According to Eq.(2.21) electron mixing angle is given by

$$\vartheta_e^2 = \frac{|z|^2}{4M_s}\cos^2\theta_{13}\left(m_1\cos^2\theta_{12} + m_2\sin^2\theta_{12} + \sin(\xi-\zeta)\sin 2\theta_{12}\sqrt{m_1 m_2}\right). \tag{2.27}$$

For $\xi - \zeta = -\pi/2$ this quantity is minimal

$$\vartheta_{e,min}^2 = \frac{|z|^2}{4M_s^2}\cos^2\theta_{13}\left(\sqrt{m_1}\cos\theta_{12} - \sqrt{m_2}\sin\theta_{12}\right)^2. \tag{2.28}$$

To compare it with the other mixing angles, we note that the relation

$$\sum_\alpha \vartheta_\alpha^2 \approx \frac{|z|^2}{4M_s}(m_1 + m_2) \tag{2.29}$$

[7] It was pointed out in [112] that both ϑ_μ and ϑ_τ can be suppress in inverted hierarchy, for $\theta_{13} = 0$. For this to happen the relation $\sqrt{\frac{m_2}{m_1}} = \tan\theta_{12}$ should hold, as one can also see from Eqs. (2.23) and (2.25). The corresponding value of θ_{12} is however well outside the 3σ interval. The general case $\theta_{13} \neq 0$ has not been analyzed in [112].

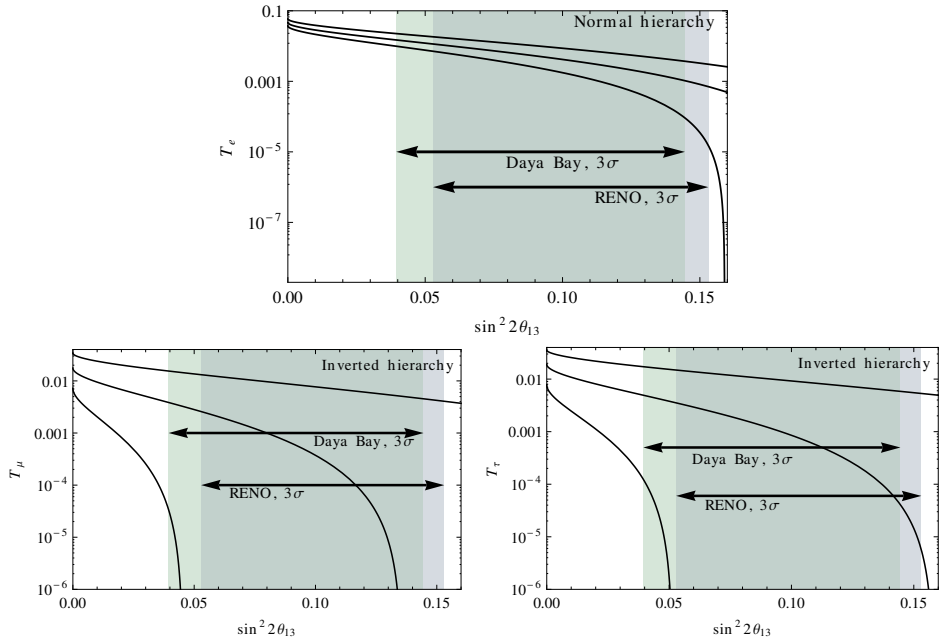

Figure 2.2: The minimal ratios of mixing angles $T_\alpha = \vartheta_\alpha^2 / \sum \vartheta_\beta^2$. **The upper** figure depicts normal hierarchy, **two lower** ones – IH. In all figures, the lower curve corresponds to the choice of the mixing angles and mass splittings that minimizes the ratio within the 3σ range, upper – that maximizes it, middle employs the best-fit parameters (for details of the choices, see Secs. 2.3.2, 2.3.3). CP-phases are $\xi = -\pi/2$ for the T_e-plot, $\phi = 0$, $\xi - \zeta = \pi/2$ for T_μ, and $\phi = \pi$, $\xi - \zeta = -\pi/2$ for T_τ. The bands *Daya Bay* and *RENO* correspond to the 3σ ranges of θ_{13}, indicated by the corresponding experiments [10, 9].

holds (similar to Eq.(2.16) in the case of normal hierarchy). Therefore

$$\frac{\vartheta_{e,min}^2}{\sum\limits_\alpha \vartheta_\alpha^2} = \frac{\cos^2\theta_{13}}{1+\frac{m_2}{m_1}} \left(\cos\theta_{12} - \sqrt{\frac{m_2}{m_1}}\sin\theta_{12}\right)^2 . \tag{2.30}$$

The results of the analysis are listed in Table 2.2 and Fig. 2.2. From the upper bound on T_α we derive the bound

$$T_\mu + T_\tau \geq 0.02 . \tag{2.31}$$

We see that in this mass hierarchy it is possible for the overall coupling of the sterile neutrino to both μ and τ flavours to become tiny compared to the electron flavour coupling.

The analysis for the inverted hierarchy was made for $|z| \gg 1$. See the Sec. 2.3.4 below for the case $|z| \sim 1$.

2.3.4 Ratio of sterile neutrino mixing angles for $|z| \sim 1$

As the expressions (2.13) and (2.21) show, the mixing angles have two terms: one is proportional to $|z|^2$ and another to $|z|^{-2}$ (recall that $|z| \geq 1$). It was shown in Sec. 2.3.3 that for inverted hierarchy the $|z|^2$-term can be zero for ϑ_μ^2 and ϑ_τ^2, while the $|z|^{-2}$ term in general stays finite.

For a given value of $|z|$, the $|z|^{-2}$-term is bounded from above. According to (2.13) and (2.21), its maximum is realized simultaneously with the maximal value of

$$L_\alpha^{NH} = |V_{\alpha 3} + ie^{i\xi}\sqrt{\frac{m_2}{m_3}}V_{\alpha 2}|^2 \tag{2.32}$$

in the normal hierarchy, and

$$L_\alpha^{IH} = |V_{\alpha 1} + ie^{i(\xi-\zeta)}\sqrt{\frac{m_2}{m_1}}V_{\alpha 2}|^2 \tag{2.33}$$

in the inverted hierarchy.

Analysis, similar to that of the Sections 2.3.2–2.3.3 shows that

$$L_e^{NH} \leq 0.2, \quad L_\mu^{NH} \leq 1.1, \quad L_\tau^{NH} \leq 1.1, \quad L_e^{IH} \leq 1.96, \quad L_\mu^{IH} \leq 1.3, \quad L_\tau^{IH} \leq 1.3\,. \tag{2.34}$$

These bounds allow to estimate the contribution of the $|z|^{-2}$-terms to the whole sum of the squared mixing angles

$$\sum_\alpha \vartheta_\alpha^2 = \frac{m_1+m_2+m_3}{4M_s}\left(|z|^2 + \frac{1}{|z|^2}\right)\,. \tag{2.35}$$

The ratio of (2.32)–(2.33) to (2.35) gives

$$R_\alpha^{NH} = \frac{L_\alpha^{NH}}{(1+\frac{m_2}{m_3})}\frac{1}{|z|^4+1}, \quad R_\alpha^{IH} = \frac{L_\alpha^{IH}}{(1+\frac{m_2}{m_1})}\frac{1}{|z|^4+1}\,. \tag{2.36}$$

For $z \sim 1$ it can become of order unity. However, we restrict ourselves to the sufficiently large values $z \gtrsim 10$, that are consistent with the upper bound, indicated by the experiments (see Fig.2.9)

$$R_e^{NH} \lesssim 2\times 10^{-5}, \quad R_{\mu,\tau}^{NH} \lesssim 10^{-4}, \quad R_e^{IH} \lesssim 10^{-4}, \quad R_{\mu,\tau}^{IH} \lesssim 5\times 10^{-5}\,. \tag{2.37}$$

Comparison these results with the *lower* bounds (Table 2.2) we see that z^{-1} terms are unimportant for the for all mixing angles in NH and ϑ_e in IH. What concerns the remaining angles ϑ_μ and ϑ_τ in IH, they can be substantially modified by account of z^{-1}-terms, but anyway each of them can become small enough, compared to the other angles, as explained in next section. As a corollary, analysis and results of Secs. 2.3.2,2.3.3 do not change significantly for large enough values of z.

2.3.5 Minimal mixing angles in the νMSM

Finally, we find the *minimal* values of the sterile neutrino mixing angles in the νMSM , compatible with the neutrino oscillation data. These angles will turn out to be much smaller than the experimental upper bounds in all regions of masses, probed by the experiments. A general solution of the see-saw equations (2.13), (2.21) gives ϑ as a function of $|z|$:

$$\vartheta_\alpha^2 = A_\alpha |z|^2 + \frac{B_\alpha}{|z|^2} \tag{2.38}$$

with coefficients A_α and B_α independent of $|z|$. The minimum of this expression is reached for $|z|_\alpha^2 = \sqrt{B_\alpha/A_\alpha} \geq 1$ and is given by

$$(\vartheta_\alpha^2)_{\min} = 2\sqrt{A_\alpha B_\alpha}. \tag{2.39}$$

To find the *absolute* lower bound on the mixing angle for a given sterile neutrino mass, we vary this expression over the parameters of neutrino oscillations. The resulting mixing angles and the corresponding values of $|z|$ are listed in Table 2.3.[8] One can see that the values presented therein do not depend significantly on the 3σ upper bound on θ_{13} that we choose. The only exception is the minimum of the ϑ_e angle. In this case the exact value of the upper bound on θ_{13} defines how close A_α, and hence $(\vartheta_\alpha^2)_{\min}$, can come to zero.

For the mixing angles $\vartheta_{\mu,\tau}^2$ in the case of inverted hierarchy $A_\alpha = 0, B_\alpha \neq 0$ and formally for infinitely large $|z|$ they would become zero. The value of $|z|$, however, is bounded from above, $|z| < z_{\max}$, by the requirement that *none of three* mixing angles exceeds its upper bound (for quantitative estimates of $z_{\max}$, look at Fig. 2.9). Therefore the couplings to μ and τ neutrinos remain *finite*. Estimates of mixing angles can be provided for B_α given by L_α^{IH} (2.33,2.34), along with $A_{\mu,\tau} = 0$, $z = z_{\max}$

$$\vartheta_{\mu,\tau}^2 \gtrsim 2 \times 10^{-8} \frac{\text{MeV}}{M_s z_{\max}^2}, \qquad \text{(IH)} \tag{2.40}$$

[8] Notice, that the ratio of the mixing angles $\vartheta_\alpha^2/\vartheta_\beta^2$ does not reach its minimum when (2.39) is satisfied. The values of $|z|$ for which the bounds on the lifetime are relaxed the most are those when some of the mixing angles reach their upper experimentally allowed value.

Flavour α	$(\vartheta^2_\alpha)_{\min}$ @ 1 MeV	$\lvert z\rvert$
e	7×10^{-10}	2.2 (2.4)
μ, τ	10^{-8}	1.5

(a) NH, best-fit

Flavour α	$(\vartheta^2_\alpha)_{\min}$ @ 1 MeV	$\lvert z\rvert$
e	10^{-10} (4×10^{-11})	6.2 (9.8)
μ	8×10^{-10} (6×10^{-10})	5.4 (6.3)
τ	1.2×10^{-9} (1.0×10^{-10})	4.6 (5.1)

(b) NH, 3σ

Flavour α	$(\vartheta^2_\alpha)_{\min}$ @ 1 MeV	$\lvert z\rvert$
e	10^{-8}	2.3
μ, τ	2×10^{-9}	3.5

(c) IH, best-fit

Flavour α	$(\vartheta^2_\alpha)_{\min}$ @ 1 MeV	$\lvert z\rvert$
e	6×10^{-9}	2.7
μ, τ	see text	

(d) IH, 3σ

Table 2.3: Minimal values of the active-sterile mixing angles ϑ^2_α, obtained using the best-fit values of neutrino oscillation parameters or by varying the neutrino oscillation data within their 3σ intervals, listed in Table 2.1. The values for $(\vartheta^2_\alpha)_{\min}$ are provided for sterile neutrinos with the mass $M_s = 1$ MeV. For other masses one should multiply them by (MeV$/M_s$). Columns "$|z|$" show the values of $|z|$ for which the minimum in (2.38) is reached. For the explanation of numbers in brackets, see Footnote 6.

2.4 Experimental bounds on sterile neutrino mixings

The direct experimental searches for neutral leptons had been performed by a number of collaborations [125, 126, 127, 128, 129, 130, 131, 132, 133, 134, 135, 136, 137] (see e.g. [108, 107] for review of various constraints). The negative results of the searches are converted into the *upper* bound on $\vartheta_\alpha \vartheta_\beta$ for different flavours. If neutrino oscillations are mediated by these sterile neutrinos, these bounds can be translated into the *upper* bounds on parameter $|z|$ and *lower* bounds on sterile neutrino lifetime.

Below, we take a closer look at two main types of experiments ("peak searches" and "fixed target experiments")[9] and describe *reinterpretation of these bounds* in

[9]The neutrinoless double-beta decay ($0\nu\beta\beta$) does not provide significant restrictions on the

the case, when sterile neutrinos with MeV–GeV masses are also responsible for neutrino oscillations.

2.4.1 Peak searches

In "*peak search*" experiments [140, 141, 142, 143], one considers the two-body decay of charged π or K mesons to charged lepton ($e^{\pm}$ or $\mu^{\pm}$) and neutrino (see e.g. [107] for discussion). In case of the pion decay the limit on ϑ_e^2 for masses in the range $60\,\mathrm{MeV} \leq M_s \leq 130\,\mathrm{MeV}$ is provided by the searches for the secondary positron peak in the decay $\pi^+ \to e^+ N$ to the massive sterile neutrino N as compared to the primary peak coming from the $\pi^+ \to e^+\nu_e$ decay. Recent analysis of [136] puts this limit at $\vartheta_e^2 < 10^{-8}$ in the mass range $60 - 129\,\mathrm{MeV}$, for earlier results see [127, 128]. In the smaller mass region ($4\,\mathrm{MeV} \lesssim M_s \lesssim 60\,\mathrm{MeV}$) Refs. [127, 128] provided the bound based on the change of the number of events in the primary positron peak located at energies $M_\pi/2$. Similar bounds were obtained for the same mixing angle in studies of *kaon* decays [131] and for the ϑ_μ^2 in the decays of both pions [133, 134, 135] and kaons [131, 132].

The *lower* bound on the sterile neutrino lifetime τ_s in the model (2.4), based on the peak search data and neutrino oscillations is shown in Fig. 2.3 by dot-dashed green lines. The parameters of neutrino mixing matrix are allowed to vary within their 3σ limits (to minimize τ_s, while still keeping the values of all mixing angles compatible with the bounds from direct experimental searches).

2.4.2 Fixed target experiments and neutral currents contribution

The second kind of experiments ("*fixed target experiments*") [126, 129, 130] aims to create sterile neutrinos in decays of mesons and then searches for their decays into pairs of charged particles. Notice, that the expected signal in this second case is proportional to ϑ_α^4 or $\vartheta_\alpha^2\vartheta_\beta^2$ (and not to ϑ_α^2 as in the case of peak searches, discussed in the Section 2.4.1). We will demonstrate below that in the models like (2.4) (and in particular in the νMSM) the results of some fixed target experiments should be reinterpreted and will provide stronger bounds than discussed in previous works [108, 107, 112] (see also [144]).

2.4.3 Reinterpretation of the PS191 and CHARM experiments

The experiment **PS191** at CERN was a "fixed target" type of experiment described above [125, 126]. In searches for sterile neutrinos lighter than the pion

parameters of the sterile neutrinos in the type-I see-saw models (contrary to the case discussed in e.g. [107]), see discussion in [112, 138]. In particular, this is the case in the νMSM [139].

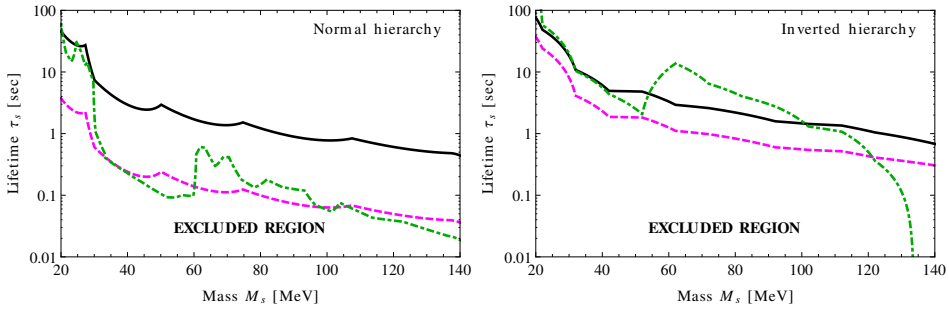

Figure 2.3: The lower bounds on the lifetime of sterile neutrinos, responsible for the mixings between active neutrinos of different flavours in the see-saw models (2.4). The bounds are based on the combination of negative results of direct experimental searches [125, 126, 128, 136, 131, 132, 133, 134, 135] with the neutrino oscillation data [123]. The neutrino oscillation parameters are allowed to vary within their 3σ confidence intervals to minimize the lifetime. The solid black curve is based on our reinterpretation of PS191 data *only*, that takes into account charged and neutral current contributions (see Sec. 2.4.3). The interpretation of the PS191 experiment, taking into account only CC interactions (used e.g. in the previous works [108, 112]) is shown in magenta dashed line. The bound from peak searches experiments *only* [128, 136, 131, 132, 133, 134, 135] is plotted in green dot-dashed line.

$M_s < M_\pi$, the pair of charged particles that were searched for in the neutrino decay comprised mostly of electron and positron:

$$\begin{aligned} \pi^+/K^+ \to e^+ + \quad & N \\ & \hookrightarrow e^+ e^- \nu_\alpha \,, \end{aligned} \tag{2.41}$$

where N is a sterile neutrino with the mass M_s. The first reaction in the chain is solely due to the *charged-current* (CC) interaction, and its rate is proportional to the ϑ_e^2.

If sterile neutrinos interact through both *charged and neutral currents* (CC+NC) as it is the case in the models with the see-saw Lagrangian (2.4), any of three active-neutrino flavours may appear in the decay of N in (2.41). The decay widths are [140]:

$$\Gamma(N \to e^+ e^- \nu_\alpha) = c_\alpha \vartheta_\alpha^2 \frac{G_F^2 M_s^5}{96\pi^3}, \tag{2.42}$$

with the following definition[10]

$$c_e = \frac{1 + 4\sin^2\theta_W + 8\sin^4\theta_W}{4}, \quad c_\mu = c_\tau = \frac{1 - 4\sin^2\theta_W + 8\sin^4\theta_W}{4}, \tag{2.43}$$

[10] Note that in the Ref. [145] there is a typo in the expression for c_τ (Eq. (2)).

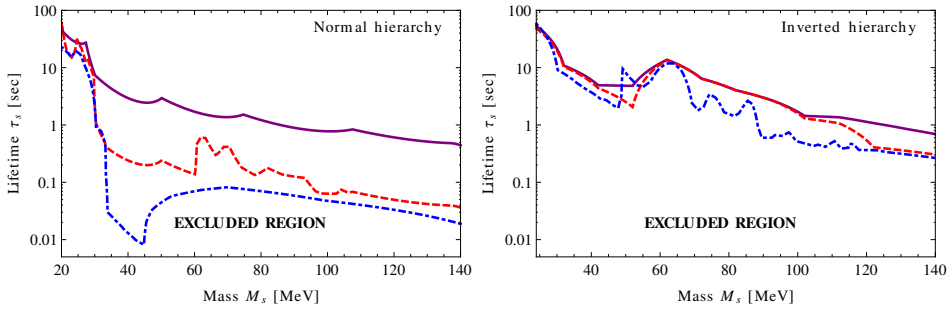

Figure 2.4: Comparison with the previous bounds on sterile neutrino lifetime in the νMSM [112]. The solid purple curves represent the results of the present analysis, obtained by the combination of peak searches experiments [128, 136, 131, 132, 133, 134, 135] together with the reanalysis of PS191, that takes into account neutral currents (a union of black and green bounds from Fig. 2.3). The red dashed curve is based on the combination of the same peak searches with the *original* interpretation of PS191 (i.e., with charged current interactions only). The blue dot-dashed line is taken from [112]. *Notice*, that the results of [112] were multiplied by a factor 2 to account for the Majorana nature of the particles (see discussion in Sec. 2.4.4), that was missing therein. The difference between the red and blue lines in the case of normal hierarchy is explained by wider 3σ intervals for neutrino oscillation data, used in [112], compared to our analysis.

and θ_W is the Weinberg's angle so that $\sin^2\theta_W \approx 0.231$ and $c_e \approx 0.59$, $c_{\mu(\tau)} \approx 0.13$. Therefore, the total number of events inside the detector that registers electron-positron pairs would be proportional to the combination of mixing angles $\vartheta_e^2 \times (\sum c_\alpha \vartheta_\alpha^2)$.

However, the model employed in the interpretation of the PS191 experiment [125, 126] was different, as has already been pointed in [144]. In the original analysis it was assumed that sterile neutrino interacts *only via charged currents*, but not through neutral currents. In our language it means that $c_e = 1, c_{\mu(\tau)} = 0$ was used instead of the values (2.43)[11]. As was noticed above, the probability of meson decay into sterile neutrino does not alter if we exclude the neutral-current interaction, and therefore the total number of events with the electron-positron pair would be proportional to $\vartheta_e^2 \times \vartheta_e^2$.

Therefore if we denote the bounds listed in [125, 126] as $\vartheta_e^4 \leq \vartheta_{e(exp)}^4$, then

[11] Model described in [125, 126] contains only one Dirac neutrino, while in the νMSM we have two Majorana fermions. Therefore actually $c_e = 1/2$ in the original model. For details see Sec. 2.4.4

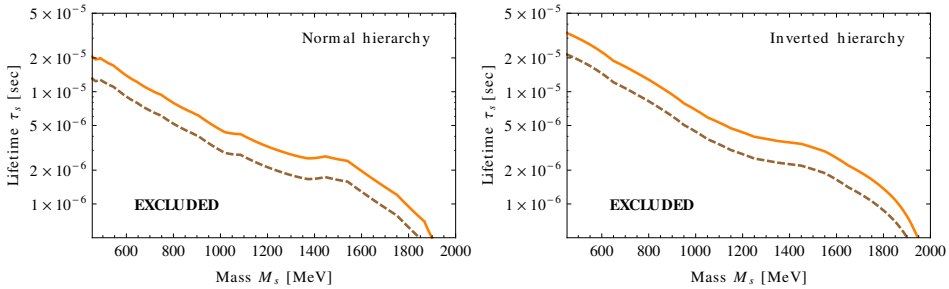

Figure 2.5: Comparison of the bounds on sterile neutrino lifetime (in the model (2.4)) based on the results of the CHARM experiments [130] *solely* (combined with the neutrino oscillation data). The orange (upper) curves correspond to the model with charged and neutral current interactions of sterile neutrinos, the brown (lower) – to the model with charged current interactions only. For details, see Sec. 2.4.3.

the bound for the νMSM takes form

$$\vartheta_e^2 \left(\sum_{\alpha=\{e,\mu,\tau\}} c_\alpha \, \vartheta_\alpha^2 \right) \leq \vartheta^4_{e(exp)} \, . \tag{2.44}$$

Similar bounds can be extracted from the reanalysis of meson decays into *muon* and sterile neutrino, that leads to replacement $e \to \mu$ in (2.44). As a result, the reinterpretation of the results of the PS191 experiment in combination with neutrino oscillation data produces up to an order of magnitude *stronger* bounds on lifetime than in the previous works (see Figs. 2.3 and 2.4).

Similarly, the CHARM experiment [130] provided bounds on the mixing angles of sterile neutrinos in the mass range $0.5\,\text{GeV} \lesssim M_s \lesssim 2\,\text{GeV}$. In the original analysis NC contributions *were neglected*. Therefore, to apply the results of this experiment to the case of the νMSM , we reanalyzed the data as described above. In Fig. 2.5 we compare lifetime bounds coming from the CHARM experiment solely for CC and CC+NC interactions of sterile neutrinos. The difference in this case is about a factor of 2.[12]

[12]In the case of the PS191 experiment, when using CC only for masses below the mass of pion suppression of the ϑ_e^2 mixing angle due to neutrino oscillations meant that instead of ϑ_e^2 bounds the lifetime is defined by the (much weaker) ϑ_μ^2 bounds. That led to the significant relaxation of the lower bound on the lifetime. If NC were taken into account, this was not possible anymore and therefore the lower bound on sterile neutrino lifetime became stronger by as much as the order on magnitude (black vs. magenta curve on the left panel in Fig. 2.3. In case of the CHARM experiment, both ϑ_e^2 and ϑ_μ^2 are strongly constrained and switching from one constraint to another makes (numerically) much smaller difference.

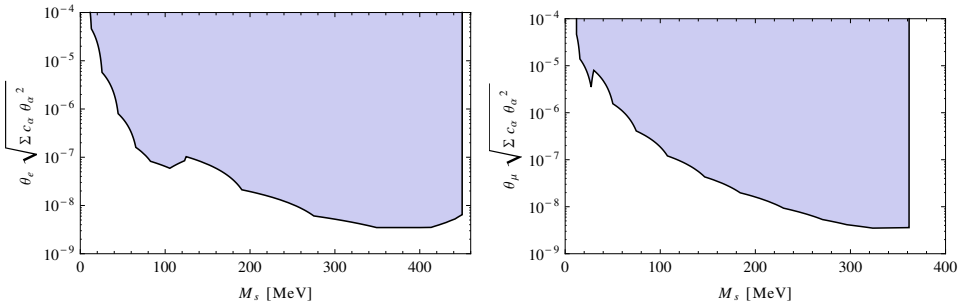

(a) Bound on the combination $\vartheta_e \sqrt{\sum c_\alpha \vartheta_\alpha^2}$ (b) Bound on the combination $\vartheta_\mu \sqrt{\sum c_\alpha \vartheta_\alpha^2}$

Figure 2.6: Direct accelerator bounds on the combination of active-sterile neutrino mixing angles, resulting from the reanalysis of the PS191 experiment [125, 126], taking into account decays of sterile neutrino through both charged and neutral currents and their Majorana nature. The shaded region is excluded. The case, analyzed in the original works [125, 126] (decay of sterile neutrino through the charged current only) corresponds to the choice $c_e = 1$, $c_\mu = c_\tau = 0$, for details, see Sec. 2.4.3. We plot the bounds for *two Majorana* neutrinos (as in Fig. 2.7) while in the original works [125, 126] a single Dirac neutrino was analyzed.

2.4.4 A note on Majorana vs Dirac neutrinos

For completeness we briefly discuss the difference in interpreting experimental results for *Majorana vs. Dirac sterile neutrinos*. Similar discussion can be found e.g. in [108]. When interpreting the experimental results one should take into account that in present analysis we consider *two Majorana sterile neutrinos*, while the experimental papers often phrase their bounds in terms of the mixing with a single *Dirac* neutrino, that we will denote U_α^2. In the νMSM twice more sterile neutrinos are produced per single reaction (because there are two sterile species – N_2 and N_3), and, owing to their Majorana nature, each sterile neutrino decays twice faster (additional charge-conjugated decay modes are present). Notice, that the mass splitting between between two sterile states N_2, N_3 is small $|M_2 - M_3| \ll \frac{1}{2}(M_2 + M_3) = M_s$ and once born, the states oscillate fast into each other. Averaging over many oscillations can be accounted for by an extra factor $\frac{1}{2}$ in the number of N_2 and N_3 species. Therefore, for fixed target experiments one gets the same number of the detector events involving one Dirac sterile neutrino as one gets in the νMSM if $(\vartheta_{\alpha 2}^2 + \vartheta_{\alpha 3}^2)^2 = U_\alpha^4$. That is, one should identify $2\vartheta_\alpha^2$ with the measured U_α^2 (recall (2.12) that $\vartheta_\alpha^2 = \frac{1}{2}(\vartheta_{\alpha 2}^2 + \vartheta_{\alpha 3}^2)$). In the case of peak searches, the bound U_α^2 should be interpreted in the νMSM as $\vartheta_{\alpha,2}^2 + \vartheta_{\alpha,3}^2 \leq U_\alpha^2$, as production of *any* state N_2 or N_3 contributes to the number of events in the secondary peak, i.e. again $2\vartheta_\alpha^2$ should be identified with U_α^2. Notice, that this factor 2 is missing in [112].

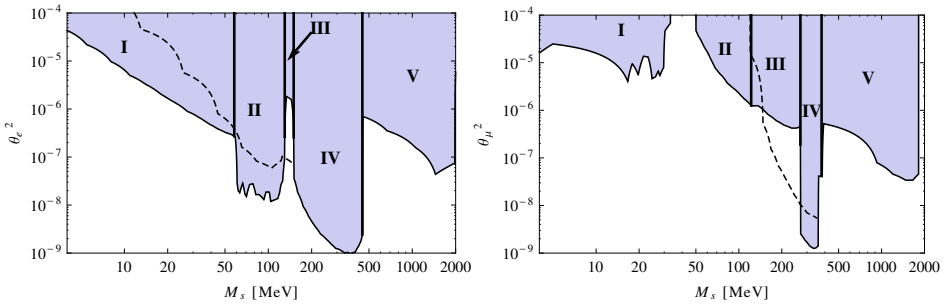

Figure 2.7: Direct accelerator bounds on the mixing angles. **Left panel:** ϑ_e^2 bounds, taken from [128] (region I), [136] (region II), [131] (region III), [126, 146] (region IV) and [130] (region V). **Right panel:** ϑ_μ^2 bounds, taken from [133, 134, 135] (region I), [131](region II), [132] (region III), [126](region IV) and [129] (region V). The shaded regions are ruled out by the experimental findings. Dashed curves indicate mixing angle bounds given by original interpretation of PS191 experiment, but we *do not* use them to derive our final results, as explained in Sec. 2.4.3. The bounds are shown for the Majorana neutrino and are therefore two times *stronger* (see Section 2.4.4), while in the original works [125, 126] a single Dirac neutrino has been considered.

2.5 Results

In this Section we summarize our results: the upper bound on the (combination of) mixing angles of sterile and active neutrinos in the see-saw models (2.1) in the range 10 MeV – 2 GeV and the lower bound on sterile neutrino lifetime, obtained in combination of these bounds with constraints, coming from neutrino oscillation data.

2.5.1 Bounds on the mixing angles of sterile neutrinos

For the models (2.4) (two Majorana sterile neutrinos, interacting through both charged and neutral interactions), the compilation of constraints on various combinations of active-sterile mixing angles (ϑ_e^2, ϑ_μ^2, $\vartheta_e\sqrt{\sum c_\alpha \vartheta_\alpha^2}$, $\vartheta_\mu\sqrt{\sum c_\alpha \vartheta_\alpha^2}$) that we used in this study are plotted in Figs. 2.6 and 2.7.[13]

2.5.2 The lower bound on the lifetime of sterile neutrinos

The result of the Sections 2.3.2–2.3.3, combined with these experimental bounds can be translated into the *lower* limits on the lifetime of sterile neutrinos. These

[13] Notice that in the published results of the PS191 experiment [126] bounds are given up to $M_s = 400$ MeV. We extend these bounds up to 450 MeV, using the PhD Thesis of J.-M. Levy [146].

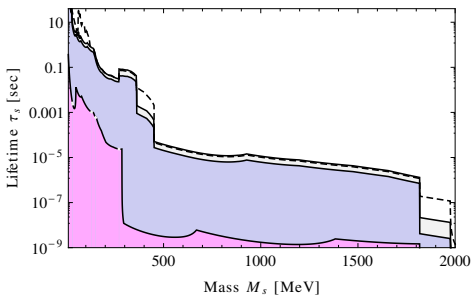

(a) Normal hierarchy, mass range 10 MeV − 2 GeV

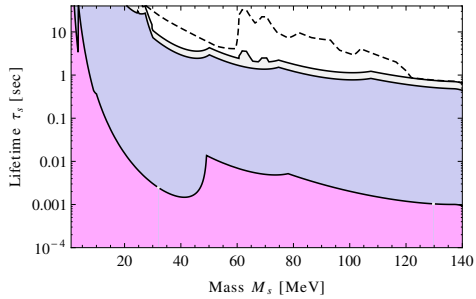

(b) Normal hierarchy, zoom at the mass range 10 MeV − 140 MeV

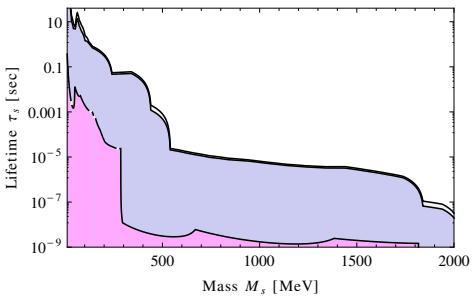

(c) Inverted hierarchy, mass range 10 MeV − 2 GeV

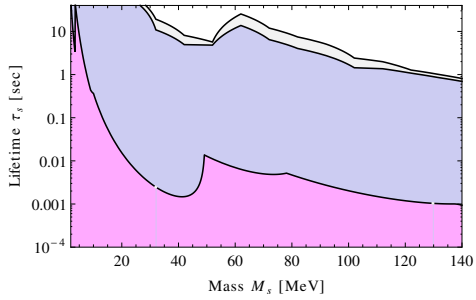

(d) Inverted hierarchy, zoom at the mass range 10 MeV − 140 MeV

Figure 2.8: The resulting lower bounds on sterile neutrino lifetime τ_s as a function of their mass, obtained by requiring that two Majorana sterile neutrinos are responsible for neutrino oscillations and their parameters do not contradict the negative results of direct experimental searches. In all figures the upper curve comes from using of the best fit neutrino oscillation parameters, the middle one – from their variation within the 3σ limits, and the lower one does not take into account neutrino oscillation data and puts all three mixing angles equal to their direct experimental bounds. The dashed line for NH corresponds to the best-fit values of PMNS parameters with $\theta_{13} = 0$ and shows how much the bounds on the lifetime relax for non-zero value of θ_{13} (see text, Section 2.5 for discussion).

results are presented in Figs. 2.8 on the preceding page. Additionally, we plot the lifetime bounds for the best-fit values of the PMNS parameters yet with $\theta_{13} = 0$ (as used e.g. in [108, 147]). For normal hierarchy we see that our bounds with $\theta_{13} \neq 0$ are relaxed by as much as the order of magnitude at some masses, compared to $\theta_{13} = 0$ case. The difference for IH is not so pronounced. *Notice*, that the bounds of [108, 147, 112] were different from what we show as dashed line in Fig. 2.8 because of ignoring the neutral current contributions to the results of PS191 experiment (for details see discussion in Section 2.4 and Figs. 2.3, 2.4).

2.6 Discussion

In this Chapter, we have investigated experimental restrictions on the parameters of the see-saw Lagrangian in the case when two sterile neutrinos with the masses between ~ 10 MeV and 2 GeV are responsible for neutrino oscillations. Combined with the results of the direct experimental searches, the neutrino oscillation data provide stringent lower bounds on their lifetime, τ_s and allows to determine both *maximum* and *minimum* values of the mixing angles ϑ_α^2.

We have reinterpreted the results of the PS191 experiment [125, 126], following [144], by taking into account not only charged, but also neutral-current interactions (as both of these are present in the Type I see-saw Lagrangian). Our results demonstrated that below the mass of the pion the fixed target experiments (ϑ^4 experiments) provide *stronger* restrictions than the peak search experiments (ϑ^2 experiments) in case of *normal hierarchy*. In *inverted hierarchy* the reanalysis of the PS191 experiment turns out to be very important as well. In the original analysis of the CHARM experiment [129] neutral-current contributions were neglected as well and we have reinterpreted these results in a similar way to PS191. The final results are presented in Figs. 2.8.

Future experiments (for example, the SHiP experiment at CERN [100, 101, 102], see Sec. 1.3.9) have a great potential of discovering light neutral leptons of the νMSM or significantly improving the bounds on their parameters (see discussion in [148] and [149]). Due to the strong suppression of the mixing angles ϑ_e^2 in the case of NH and ϑ_μ^2 in the case of IH, the peak searches in the kaon decays (such as e.g. [150]) may miss the sterile neutrino (cf. [112]).[14]

As we have discussed in Sec. 1.3.3, the out-of-equilibrium behaviour of sterile neutrinos may lead as well to the successful baryogenesis scenario [153, 119, 147]; the generation of large lepton asymmetry at temperatures below the sphaleron freeze-out [109]. In Fig. 2.9 we superimpose the bounds on $|z|$, coming from the direct experimental searches on the region of parameters ($|z|$, M_s) in which the successful baryogenesis is possible (the region inside the black contours marked "BAU" based on the Ref. [147]).

[14] GeV-scale sterile neutrinos in the models with extended Higgs sector [151] can be searched at the LHC [152].

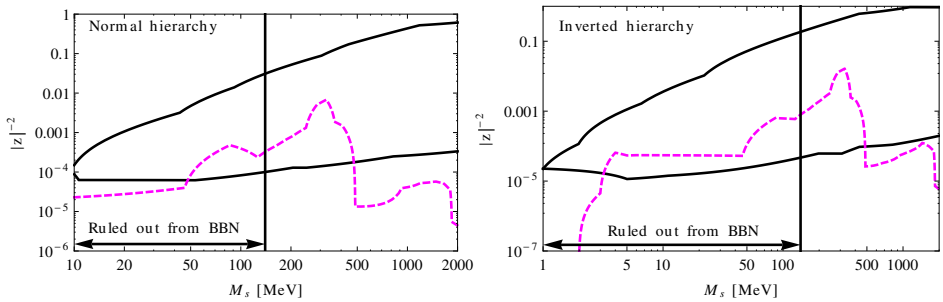

Figure 2.9: The region of successful baryogenesis in the νMSM compared with the experimental upper bounds on the parameter $|z|$. The vales of M_s and $|z|$, lying inside the black solid lines lead to the production of the observable baryon asymmetry (from [147]). The magenta dashed line marks is the *lower* bound on $|z|^{-2}$ (parameter, called ϵ in [109, 147]) such that for smaller values at least one of the mixing angles ϑ_α^2 is in contradiction with direct experimental searches (for the best-fit values of the PMNS mixing angles and masses). The value of $|z|$ corresponding to the bound is what we refer to as $z_{\max}$ in Sec. 2.3.5. The region to the left of $M_s = 140\,\mathrm{MeV}$ is ruled out from comparison with primordial nucleosynthesis bounds (Fig. 3.13).